Magazine of Civil Engineering

ISSN 2712-8172

journal homepage: http://engstroy.spbstu.ru/

Research article

UDC 69

DOI: 10.34910/MCE.129.8

Concrete beams reinforced with longitudinal and transverse GFRP bars

S.A. Mohammed ✉, ***A.I. Said***

The University of Baghdad, Baghdad, Iraq

✉ *shaysh96@outlook.com*

Keywords: GFRP, flexure, deflection, crack, concrete, shear, dowel action

Abstract. This research investigated experimentally and numerically the general behavior of six concrete beams reinforced with longitudinal and transverse bars made of Glass Fiber Reinforced Polymer (GFRP) or steel. Six beams were divided into three groups with different variables. The first group consisted of two beams reinforced with GFRP bars in main direction and with steel stirrups. The variable of this group was the spacing between the stirrups. The second group consisted of two beams also reinforced with GFRP bars in the longitudinal direction and with stirrups in the transverse direction. The variable of this group was the same – spacing between the stirrups. As for the third group, it consisted of two beams reinforced with GFRP bars in the longitudinal direction and without stirrups in the transverse direction. The variable of this group was the main reinforcement ratio. The results showed that the beams reinforced with GFRP bars improved their behavior, bending strength and the deflection with different ratios, but had somewhat limited shear resistance when using GFRP stirrups. All the tested beams exhibited linear elastic behavior until failure, with GFRP being more brittle compared to that of ductile steel. The numerical simulation of six beams using ABAQUS software showed good agreement with the experimental data obtained in the laboratory.

Citation: Mohammed, S.A, Said, A.I. Concrete beams reinforced with longitudinal and transverse GFRP bars. Magazine of Civil Engineering. 2024. 17(5). Article no.12908. DOI: 10.34910/MCE.129.8

1. Introduction

Concrete and steel are foundational materials in construction, renowned for their strength and durability. However, given the widespread use of these materials, the search for superior alternatives has become essential. Fiber Reinforced Polymer (FRP), particularly Glass Fiber Reinforced Polymer (GFRP), has emerged as a promising substitute due to its advantageous properties over steel. GFRP is lightweight, possesses higher tensile strength than steel, and is resistant to magnetic fields, making it especially suitable for civil engineering applications [1–4]. Bank, L.C. [5] discussed FRP's potential to extend the lifespan of structures in harsh environments, while Saraswathy, T. et al. [6] investigated the flexural behavior of reinforced concrete beams using GFRP bars. Their study explored parameters, such as failure mode, crack pattern, load carrying capacity, load deflection behavior, and ductility in GFRP-reinforced concrete beams. GFRP materials offer advantages, such as corrosion resistance and a high strength-to-weight ratio, making them suitable for reinforced concrete applications where conventional steel reinforcement faces serviceability issues. Ahmed, A. et al. [7] further validated the superior performance and cost-effectiveness of GFRP-reinforced concrete beams. GFRP addresses critical challenges, such as steel corrosion, which compromises structural integrity and increases maintenance costs. Its corrosion resistance, lightweight nature, and electromagnetic neutrality make GFRP ideal for applications in marine infrastructure, MRI centers, and electrical substations [8]. Despite these advantages, the long-term performance of GFRP-reinforced structures requires further study. According to the ACI 440.IR-15 guidelines [9], GFRP-reinforced concrete beams should be over-reinforced to fail by concrete crushing rather than bar rupture. The flexural behavior of these beams is less ductile due to the linear elastic and brittle nature of GFRP bars until failure.

The aim of this study is to evaluate the structural performance of concrete beams reinforced with GFRP bars, focusing on their flexural behavior, shear resistance, and the effects of varying stirrup configurations. Specifically, the study investigates how increasing the number of GFRP stirrups impacts load-bearing capacity and deflection, and compares the performance of GFRP to steel reinforcement. Through this research, the study seeks to contribute to the development of optimized design practices for integrating GFRP in construction.

2. Methods

2.1. Specifications of the Beams under Test

The experimental program consisted of testing six beams under four-point loading. The beams were divided into three groups with different variables, such as the main reinforcement ratio, the distances between the stirrups, as well as the stirrup type used to reinforce the beams (steel or GFRP). All beams had the same dimensions of 2700 mm in length, 180 mm in width, and 260 mm in depth, with the clear span of 2500 mm. The first group included two beams reinforced with GFRP bars in the main direction and steel stirrups in the transverse direction, labeled B.S1 and B.S3. The second group included two beams reinforced with GFRP bars in the longitudinal direction with GFRP stirrups in the transverse direction, labeled B.G1 and B.G3. The third group included two beams reinforced with GFRP bars in the main direction without stirrups, labeled G1 and G3. Fig. 1 and Table 1 show the details of all the tested beam specimens.

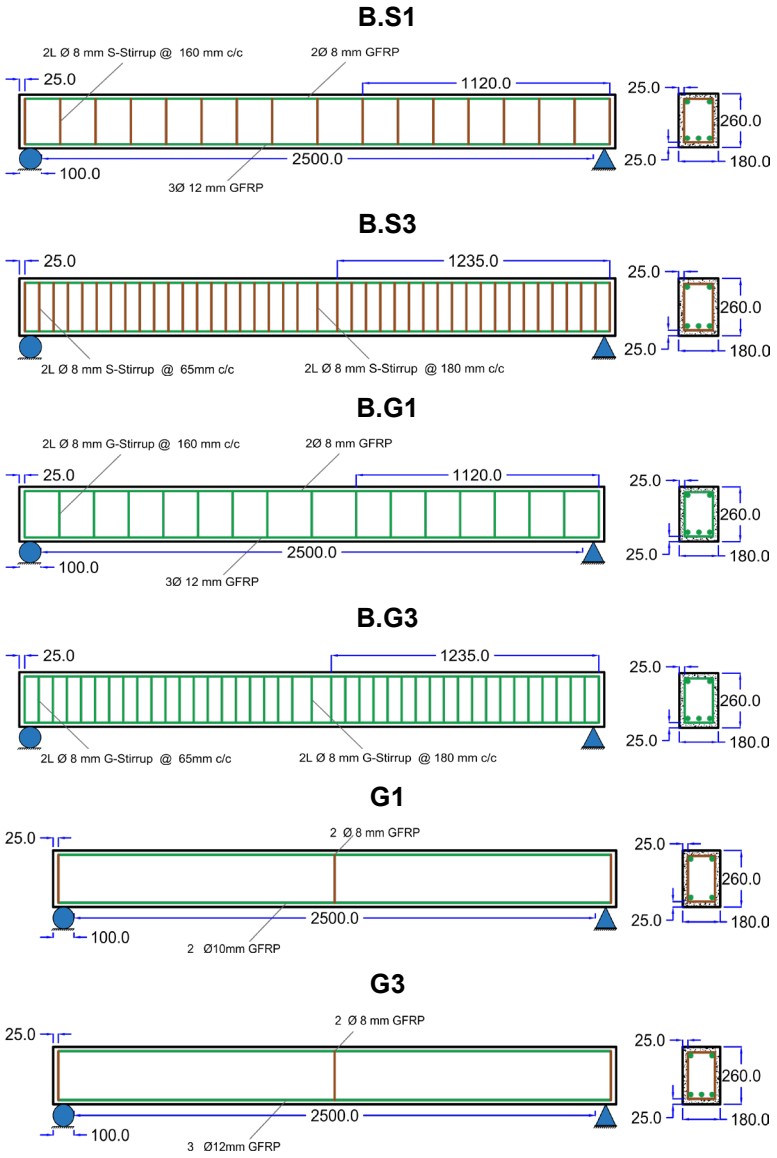

Figure 1. Details of all tested beams.

Table 1. Details of reinforcement of the beams.

Groups	Sample	Spacing	Type of stirrups	Bar top	Bar bottom
Group 1	B.S1	160 mm	Steel – Ø 8 mm	2 Ø 8 mm	3 Ø 12 mm
	B.S3	65 mm	Steel – Ø 8 mm	2 Ø 8 mm	3 Ø 12 mm
Group 2	B.G1	160 mm	GFRP – Ø 8 mm	2 Ø 8 mm	3 Ø 12 mm
	B.G3	65 mm	GFRP – Ø 8 mm	2 Ø 8 mm	3 Ø 12 mm
Group 3	G1	N/A	N/A	2 Ø 8 mm	2 Ø 10 mm
	G3	N/A	N/A	2 Ø 8 mm	3 Ø 12 mm

*N/A: not applicate

2.2. Material Properties

2.2.1. Concrete mix design

The concrete mix was designed according to ACI 211.1-22 guidelines [10] to achieve a compressive strength of 40 MPa. This concrete mix consisted of sand, gravel, cement, water, and some chemical additives to increase workability without affecting the strength of the hardened concrete. Table 2 shows the concrete mix proportions for one cubic meter of this material.

Table 2. Proportions of the concrete mix components.

Cement, kg/m^3	Gravel, kg/m^3	Sand, kg/m^3	Water, liter/m^3	Silica, kg/m^3
475	1030	640	170	20

2.2.2. GFRP bars

The longitudinal reinforcement consisted of GFRP bars of 8, 10, and 12 mm diameters. The stirrups are closed loops made of GFRP with 8 mm diameter. Several tensile tests were carried out on GFRP bars as shown in Fig. 2, for different diameter, and the results showed high tensile strength. The tensile tests were carried out in accordance with the ISO10406-1 specifications [11]. According to ISO requirements, a number of steel tubes of different diameters and fixed lengths, as shown in Fig. 2, were manufactured. GFRP bars were inserted into these tubes using epoxy adhesive from Sika Company (Sika AnchorFix®-3030), as shown in Fig. 2, because, due to their high tensile strength, the GFRP bars may fall out of the tensioning machine during testing. The manufacturer's manual reported a modulus of elasticity of 70000 MPa for all GFRP bars. Table 3 shows the results of the tensile tests on GFRP bars. The Laboratories of the Consulting Office at the College of Engineering, University of Baghdad, conducted all the tensile test.

Figure 2. Details of tensile strength test.

Table 3. Results of the tensile strength test of GFRP bar.

Type of bar	Ultimate tensile strength, MPa	Yield strength, MPa
GFRP	1350	N/A

*N/A: not applicate

2.3. Testing Procedure

The laboratory setup for the test consisted of a frame with supports spaced according to the design specifications. The specimen geometry specifications were 2700 mm long, 2500 mm span between the supports, and the width of support is 100 mm. Welded supports held up the specimens. Rubber pads and spirit level were used to level and stabilize these specimens. The concrete beam model was painted with a light white color to enhance the visibility of cracks during the test. After that, strain gauges were installed in bending and shear areas as well as an LVDT. After that, the specimen was lifted and placed on the frame, and the hydraulic jack and the load cell were installed on the I-section. The measuring devices were connected to the computer and data logger. A simple preliminary test was performed to verify the readings

of the strain gauges and the LVDT. The specimen was tested by applying an incremental load of 250 kg per stage until the hydraulic jack failed. The concrete beam was monitored during the test to determine the cracks formation from an incremental load. The cracks were marked with black lines along with the corresponding load values. All test results were recorded by the data logger in the form of tables, containing hundreds of thousands of data until the ultimate failure of concrete beams. Fig. 3 shows the details of the test setup components.

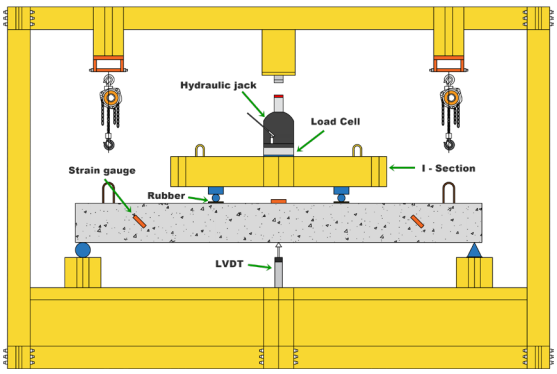

Figure 3. Details of the test setup components.

2.4. Finite Element Simulation

To gain a better understanding of the behavior of GFRP and obtain reliable scientific results, the beams were modeled using ABAQUS and a variety of theories to simulate four-point bending. The models of the materials used were determined by their properties and the adopted theories that were divided into two parts. The first part involved the representation of concrete using the concrete damaged plasticity model, similar to the smeared cracking model but more accurate. The second part involved the representation of steel using the classical theory of metal plasticity. This concept is based on the well-known von Mises yield criterion [12]. The beam components included GFRP, steel, stirrups, as well as a set of bearing plates. These components were assigned the material properties defined in the property field where the elastic behavior of concrete and the plastic behavior of concrete damage were specified. After that, elasticity and plasticity for GFRP and steel were defined, and the modulus of elasticity and Poisson's ratio were also defined for concrete. The bearing plates were assumed to be made of elastic steel. In next phase of the modeling process, the beam components were assembled, and the static loads applied to the beams were defined. The nature of the bond between GFRP and concrete was assumed to be ideal, and the interaction between all beam sections was described. After that, the loads and constraints for roller and hinge supports were also defined. There were some attempts to find the optimal mesh size and shape during the meshing phase, with generally good results.

2.4.1. Bar properties

Due to their high tensile strength and low elastic modulus, GFRP bars exhibit brittle behavior and unexpected failure, but the modulus of elasticity in steel is higher. The manufacturer characteristics of GFRP and steel bars are shown in Table 4.

Table 4. The manufacturer characteristics of GFRP and steel bars.

Type of Bar	Tensile strength f_y	Rupture strain ε	Modulus of elasticity E
GFRP	1350 MPa	0.0192	70000 MPa
Steel	510 MPa	0.0025	200000 MPa

2.4.2. ABAQUS parameters

The finite element theories rely on parameters that reflect the general properties of concrete in its common state. These parameters were determined by extensive research and investigations on concrete behavior [13]. Concrete damage plasticity data used in models are shown in Table 5.

Table 5. Concrete damage plasticity.

Parameters	ψ	ϵ	fb0/fc0	K	μ
Values	45	0.1	1.17	0.668	0.0001

3. Results and Discussion

The result of testing the six concrete beams showed good resistance to bending loads. As well, the deflection has decreased. The resistance of GFRP to shear forces was somewhat limited. The failure patterns and the number of cracks were affected by changing the spacing between the stirrups, in addition to that the type of the stirrups also had a significant impact on the stiffness of the beams, as the ability of the beam to carrying loads increased significantly with the increase in the number of stirrups, in addition to significantly reducing the spacing between the stirrups also contributed to changing the pattern failure. In terms of the longitudinal reinforcement, the deflection decreased as the proportion of the longitudinal reinforcement increased due to the effect of dowel action, and the resistance of beams to shear forces increased as the proportion of the main reinforcement improved [14].

3.1. Cracks Patterns and Fracture Mode

The first group of beams consisted of two beams that were reinforced with GFRP in the longitudinal direction as a main reinforcement in the same ratio for all beams ($1.5\,\rho_b$) and with steel stirrups in the transverse direction with different spacing (160 and 65 mm), which is the main variable for this group. In beam B.S1, the first crack appeared vertically (at an angle of 90°) in the tension area at a load of 15 kN between the two loading points in the mid-span, which is about 10.35 % of the ultimate load capacity. The cracks began to spread to the right and left in equal measure in the bending moment area until the model failed suddenly at a load of 145 kN. The sudden failure was caused by the concrete collapsing before the GFRP bars ruptured in the tension zone, which is known as compressive failure.

In B.S3 beam, the first cracks were also vertical and occurred in the tension zone at a load of 15 kN as well, 8.9 % of the ultimate load capacity. In this model, the spacing between stirrups was decreased by 59.3 % from that of the B.S1 beam. The increase in the stirrups by narrowing the spacing between them led to an increase in bearing capacity of beam by 16.5 % compared to the B.S1. The beam failed suddenly at a load of 168 kN. Concrete collapsing followed by the GFRP bars rupture directly in the compression zone. This beam was stiffer because the distance between the steel stirrups was reduced by a larger percentage than in the beam B.S1. Hence, higher bearing capacity in addition to smaller crack width and fewer cracks. Fig. 4 shows the crack pattern of the tested beams of the first group.

Figure 4. Crack pattern of the beams B.S1 and B.S3.

The second group also included two beams that have been over-reinforced to resist tensile forces with GFRP stirrups to resist shear forces. These beams were reinforced with GFRP bars in the longitudinal direction as the main reinforcement. The primary variable in this group was spacing (160 and 65 mm) between the GFRP stirrups, and the main reinforcement was a constant ratio ($1.5\,\rho_b$) in all beams. Due to the use of stirrups made entirely of GFRP, the pattern of cracks and failures in this group differed from that of the first group. The first crack in the beam B.G1 appeared in the tension region between two loading points at a load of 15 kN, 12.8 % of the ultimate load capacity. The cracks continued to increase in width and length in the bending moment area and started to spread diagonally at a distance (d) from the support face at a 45° oblique angle in the shear zones. These cracks persisted in the shear zone until the beam suddenly failed at a load of 117 kN, at which point the concrete in this zone collapsed and the GFRP stirrups ruptured, followed by splitting in the concrete cover. When compared to B.S1, this beam showed that the stirrups made of GFRP are generally weak in compression and have low elastic modulus compared to stirrups made of steel. This caused the failure pattern for B.S1 to change from compression failure to shear failure in B.G1. Because the GFRP stirrups weakly confine the concrete to the beam compared to steel stirrups, splitting in the concrete was also present in this beam.

The failure pattern of B.G3 beam differed from that of the previous beam. In the compression zone close to the loading zone, where this model failed due to sudden collapsing of the concrete, a condition

known as compression failure at a load of 142 kN occurred. The first vertical crack appeared at a load of 17.5 kN, 12.3 % of the ultimate load capacity, in the tension zone. The cracks spread between the two loading points in the bending moment area until the model failed due to compression. Due to excessive and further confinement of the beam, the failure pattern changed from shear to compression, and the distance between the stirrups became 59.3 % smaller than in the model B.G1. Thus, the addition of more stirrups along the beam increased its capacity to resist shear forces and changed its failure pattern.

The probability of large diagonal cracks in the shear zones or splits in the concrete cover, as occurred with previous beams of the same group, was significantly reduced as a result of the increase in the number of stirrups and the bonding strength between GFRP bars and the concrete. By reducing the beam size, the number of cracks and their width were significantly reduced. Fig. 5 shows the crack pattern of beams of the second group.

Figure 5. Crack pattern of the beams B.G1 and B.G3.

In the third group of beams, shear is the main cause of failure. In the model G1, the first crack appeared at a load of 10 kN, which is about 11 % of the ultimate load capacity, between the two loading points in the mid-span. Directly below the two loading points, cracks continued to develop and grew in length and width. At a load of 35 kN, the cracks began to tilt slightly and spread clearly in an oblique pattern beyond the two loading points on the right and left. When the load was 91 kN and the angle was 45 degrees, shear failure suddenly occurred. The cracks continued to branch in the shear zones and spread diagonally. Horizontal sliding and slight splitting of the concrete cover along the beam illustrates the pattern of failure in this beam. The longitudinal reinforcement with GFRP bars, which was used to resist shear forces, caused splitting in the concrete cover.

In beam G3, the first crack appeared at a load of 7.5 kN, which is about 6.3 % of the ultimate load capacity. First crack appeared vertically between the two loading points. Cracks began to spread in the bending moment area and increased in length and perpendicularity at a load of 20 kN. At a load of 35 kN, cracks began to increase below the loading points on the left and right and spread slightly obliquely. At a load of 70 kN, cracks began to spread in the shear zones. Then, the crack widths began to increase gradually in the shear zones near the supports as the applied load increased, and this was followed by a horizontal crack in the concrete cover beneath the bottom of the beam. This beam exhibited the effect of dowel action, wherein the longitudinal GFRP bars resisted a portion of the shear forces in the beam via dowel action, which had a greater effect than in beam G1. By increasing the ratio of longitudinal GFRP bar reinforcement by 200 % compared to beam G1, the resistance of the beam to shear forces increased by about 29.6 %. The failure pattern consisted of cracking of the concrete cover, an increase in diagonal cracks on both sides of the beam, and a sudden shear failure at a load of 118 kN. Fig. 6 shows the crack pattern of beams of the third group.

Figure 6. Crack pattern of the beams G1 and G3.

3.2. Load–Deflection

The four-point bending test of the concrete beams involved measuring the load and the midspan displacements at each loading stage. The resulting load–displacement curves revealed a distinct behavior for the beams reinforced with GFRP bars compared to those with all-steel bars. The GFRP-reinforced beams exhibited larger deflections than the steel reinforced beams, regardless of the orientation of the GFRP bars. This can be attributed to the lower elastic modulus of the GFRP bars relative to the steel bars. The service load deflections were also higher for the GFRP-reinforced beams than for the steel-reinforced beams. Thus, GFRP-reinforced concrete beams should be designed with serviceability criteria (deflection and cracks) in mind due to its low modulus of elasticity [15–19]. The type of stirrups, whether GFRP or steel, had barely noticeable impact on the load–displacement curves.

The first group's main variable was steel stirrup spacing. The maximum service load for this group was 60 % of B.S3 beam. Load–deflection curves showed that increasing the number of steel stirrups by gradually reducing their spacing did not affect deflection much as shown in Fig. 7. At service load, B.S1 beam deflection was 15 % lower than that of B.S3. Despite the densification of the steel stirrups, the longitudinal reinforcement ratio with GFRP bars in three beams remained constant, limiting beam deflection. As can be seen from the curves, increasing the number of steel stirrups in the beams increased their load-bearing capacity. The beams failed linear elastic and brittle.

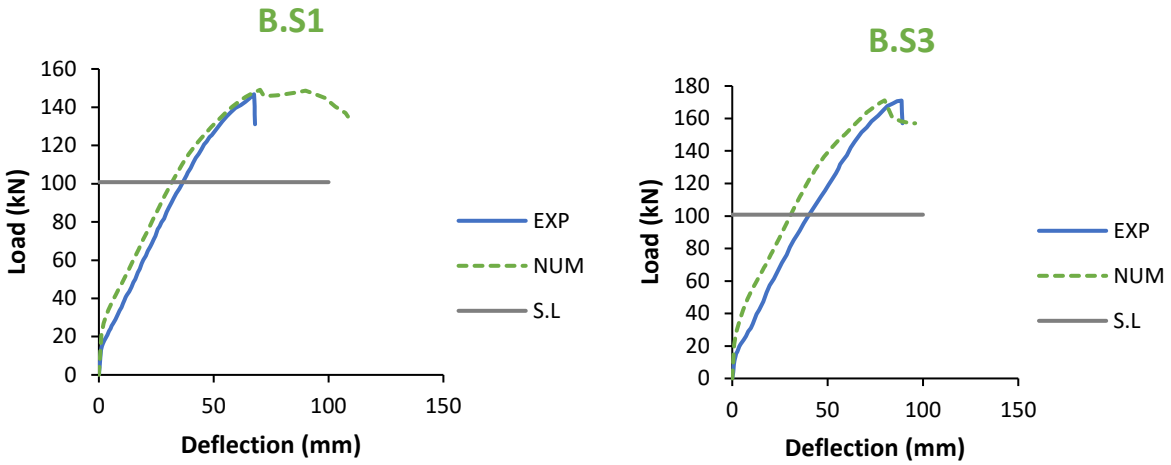

Figure 7. Load–deflection curves for B.S1 and B.S3 beams.

The maximum service load for the second group was the same – 60 % of B.G3 beam. As shown in Fig. 8, increasing the number of GFRP stirrups in concrete beams only slightly affected deflection. Reducing the spacing between them resulting in beam B.G3 deflecting 9.4 % less than B.G1 beam at service load. The deflection was not affected by the spacing between stirrups, but it did affect the pattern of failure in the beams and their capacity to support loads. The curves below show that the beams exhibit linear elastic behavior until failure. In contrast to ductile steel, the beams failed brittle and linearly.

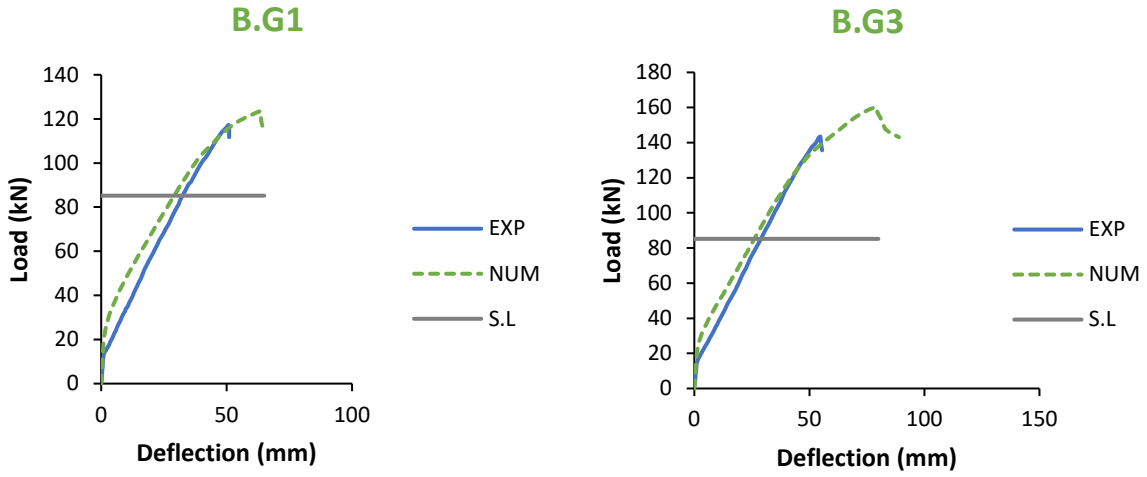

Figure 8. Validation of load–displacement for (B.G1 & B.G3) beams.

The service load ratio in the third group was approximately 60 % of the ultimate load for G3. According to the load–deflection results shown in Fig. 9, increasing the longitudinal reinforcement ratio has contributed to a significant reduction in deflection in G3 beam at service load compared to that of model G1. The curves below show that the deflection in the G3 model is 52 % less than that of model G1 as a result of the increase in the main reinforcement ratio. Increasing the main reinforcement ratio increased the ultimate load bearing capacity of the beams. The behavior of the beams reinforced with GFRP bars under the influence of loads was linear elastic until failure, indicating that the beam exhibited brittle behavior, in contrast to behavior of beams reinforced with steel bars, which was more ductile.

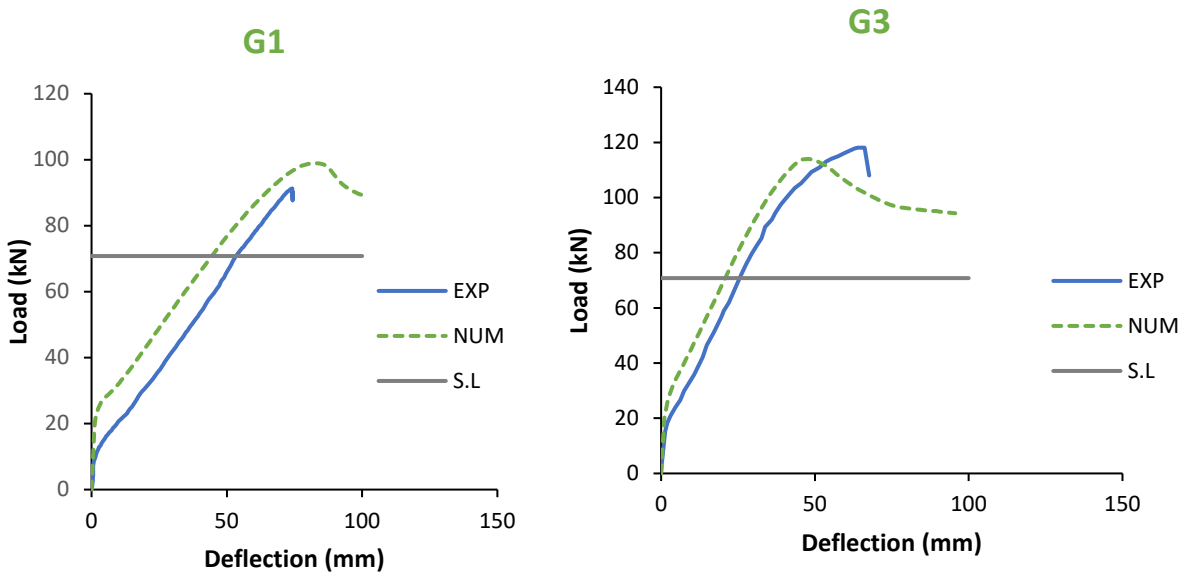

Figure 9. Validation of load–displacement for (G1 & G3) beams.

3.3. Numerical Results

The numerical values showed high consistency and accuracy with the experimental data regarding beam load-bearing capacity and ultimate deflection. The numerical validation revealed that the load–deflection curves had a similar trend to the experimental results. Moreover, the failure mode was also consistent between the experimental and numerical aspects. The results showed that the finite element method (FEM) was more rigid than the experiment test data [20]. The ultimate loads obtained from the experimental test were lower than the final loads obtained from the finite element analysis (FEA), which were significantly higher. These differences were within an acceptable range, and as a result, the FEM could be used for further studies by changing the parameters in question. The agreement between experimental and numerical results in load–deflection was good as shown in the previous curves. The results of the numerous analyses in the ABAQUS program were based on a number of theories and attempts to achieve this accuracy and agreement between the results for the experimental and numerical sides. Since the GFRP had lower compressive strength than the tensile strength, each element in the concrete beams was modeled according to its properties and in a way that is closer to the experimental side. It is worth noting that the GFRP stirrups were modeled in a solid form in order to take the changes in three directions, not only in compression and tension, and for the results to be as realistic as possible [21–25]. Fig. 10 shows the crack pattern of all tested beams using ABAQUS software.

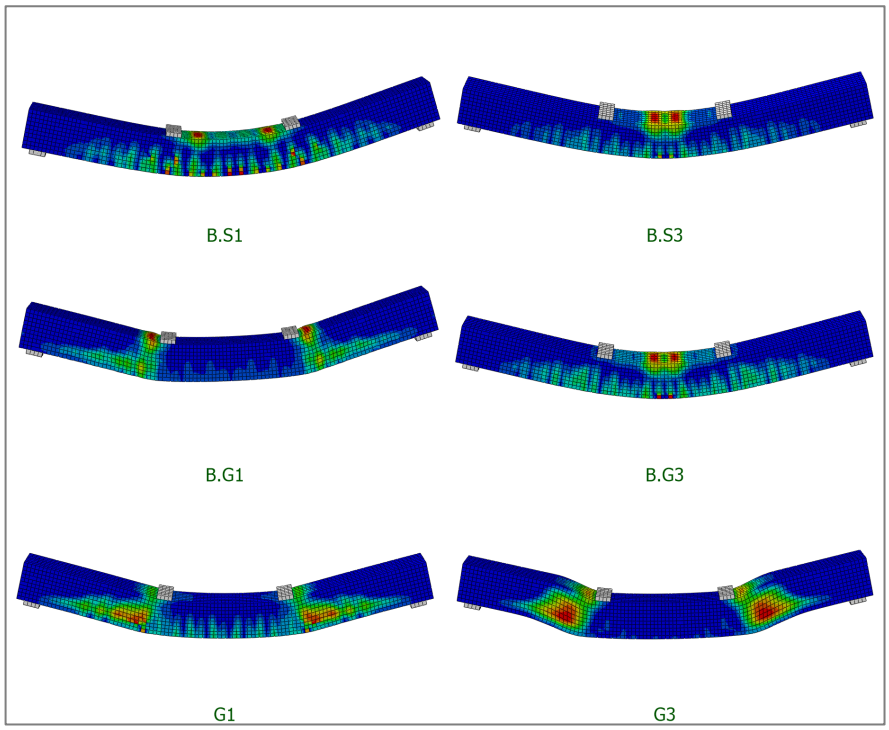

Figure 10. Crack pattern of all tested beams modeled using ABAQUS software.

4. Conclusions

- The results showed that the beams reinforced with GFRP bars exhibited linear elastic and brittle behavior until failure, whereas the beams reinforced with steel bars displayed ductile behavior with. This was attributed to the low modulus of elasticity of GFRP bars compared to the high modulus of elasticity of steel bars.
- Increasing the number of steel stirrups by reducing the spacing between them did not significantly affected deflection, but it contributed to increasing the stiffness of the beam as well as increasing the ability of the beam to bear the bending loads by 16.5 %.
- The resistance of the GFRP stirrup to shear forces was limited compared to the steel stirrup, but the increase in the number of stirrups led to making the beam more confined, and thus the failure pattern shifted from shear failure to compression failure.
- Increasing the number of GFRP stirrups increased the beam capacity to bear loads by 21.4 % and reduced the deflection by 9.4 %. However, increasing the number of steel stirrups at beam B.S3 by a large percentage contributed to increasing deflection because the weight of GFRP is lighter than that of steel.
- By adding more GFRP bars to the main reinforcement, the beam was able to resist shear forces by 29.6 % and reduced deflection by 52 % because of the dowel action effect.

References

1. Said, A.M.I., Abbas, O.M. Evaluation of Deflection in High Strength Concrete (HSC) I-Beam Reinforced with Carbon Fiber Reinforced Polymer (CFRP) Bars. The 7th Asia Pacific Young Researchers and Graduates Symposium “Innovations in Materials and Structural Engineering Practices”. Kualapor, 2015. Pp. 519–533.
2. Said, A.M.I., Tu’ma, N.H. Numerical Modeling for Flexural Behavior of UHPC Beams Reinforced with Steel and Sand-Coated CFRP Bars. IOP Conference Series: Earth and Environmental Science. 2021. 856(1). Article no. 012003. DOI: 10.1088/1755-1315/856/1/012003
3. Said, A.I., Abbas, O.M. Serviceability behavior of high strength concrete I-beams reinforced with carbon fiber reinforced polymer bars. Journal of Engineering. 2013. 19(11). Pp. 1515–1530. DOI: 10.31026/j.eng.2013.11.01
4. Ali, S.I., Allawi, A.A. Effect of web stiffeners on the flexural behavior of composite GFRP-concrete beam under impact load. Journal of Engineering. 2021. 27(3). Pp. 73–92. DOI: 10.31026/j.eng.2021.03.06
5. Bank, L.C. Composites for Construction: Structural Design with FRP Materials. John Wiley & Sons, 2006. 576 p.
6. Saraswathy, T., K. Dhanalakshmi. Investigation of Flexural Behaviour of RCC Beams using GFRP Bars. International Journal of Scientific & Engineering Research. 2014. 5(1). Pp. 333–338.
7. El-Nemr, A., Ahmed, E.A., El-Safty, A., Benmokrane, B. Evaluation of the flexural strength and serviceability of concrete beams reinforced with different types of GFRP bars. Engineering Structures. 2018. 173. Pp. 606–619. DOI: 10.1016/j.engstruct.2018.06.089

8. Emparanza, A.R., Kampmann, R., De Caso, F., Morales, C., Nanni, A. Durability assessment of GFRP rebars in marine environments. Construction and Building Materials. 2022. 329. Article no. 127028. DOI: 10.1016/j.conbuildmat.2022.127028
9. Guide for the design and construction of structural concrete reinforced with FRP bars. ACI 440.1R-15. American Concrete Institute (ACI), 2015. 88 p.
10. Selecting proportions for normal-density and high density-concrete – guide. ACI PRC-211.1-22. American Concrete Institute (ACI), 2022.
11. Fibre-reinforced polymer (FRP) reinforcement of concrete – Test methods – Part 1: FRP bars and grids. ISO 10406-1:2015. International Organization for Standardization (ISO), 2015. 39 p.
12. Besseling, J.F. A theory of Elastic, Plastic, and Creep Deformations of an Initially Isotropic Material Showing Anisotropic Strain-Hardening, Creep Recovery, and Secondary Creep. Journal of Applied Mechanics. 1958. 25(4). Pp. 529–536. DOI: 10.1115/1.4011867
13. Genikomsou, A.S., Polak, M.A. Finite element analysis of punching shear of concrete slabs using damaged plasticity model in ABAQUS. Engineering Structures. 2015. 98. Pp. 38–48. DOI: 10.1016/j.engstruct.2015.04.016
14. Yost, J.R., Gross, S.P., Dinehart, D.W. Shear Strength of Normal Strength Concrete Beams Reinforced with Deformed GFRP Bars. Journal of Composites for Construction. 2001. 5(4). Pp. 268–275. DOI: 10.1061/(ASCE)1090-0268(2001)5:4(268)
15. Lin, X., Zhang, Y.X. Bond-slip behaviour of FRP-reinforced concrete beams. Construction and Building Materials. 2013. 44. Pp. 110–117. DOI: 10.1016/j.conbuildmat.2013.03.023
16. Murthy, A.R., Pukazhendhi, D.M., Vishnuvardhan, S., Saravanan, M., Gandhi, P. Performance of concrete beams reinforced with GFRP bars under monotonic loading. Structures. 2020. 27. Pp. 1274–1288. DOI: 10.1016/j.istruc.2020.07.020
17. Ibrahim, T.H., Allawi, A.A. The Response of Reinforced Concrete Composite Beams Reinforced with Pultruded GFRP to Repeated Loads. Journal of Engineering. 2023. 29(1). Pp. 158–174. DOI: 10.31026/j.eng.2023.01.10
18. Mohammed, S.A., Said, A.I. Analysis of concrete beams reinforced by GFRP bars with varying parameters. Journal of the Mechanical Behavior of Materials. 2022. 31(1). Pp. 767–774. DOI: 10.1515/jmbm-2022-0068
19. Ali, H.H., Said, A.M.I. Flexural behavior of concrete beams with horizontal and vertical openings reinforced by glass-fiber-reinforced polymer (GFRP) bars. Journal of the Mechanical Behavior of Materials. 2022. 31(1). Pp. 407–415. DOI: 10.1515/jmbm-2022-0045
20. Allawi, A.A., Ali, S.I. Flexural Behavior of Composite GFRP Pultruded I-Section Beams under Static and Impact Loading. Civil Engineering Journal. 2020. 6(11). Pp. 2143–2158. DOI: 10.28991/cej-2020-03091608
21. Raza, A., Khan, Q.Z., Ahmad, A. Numerical Investigation of Load-Carrying Capacity of GFRP-Reinforced Rectangular Concrete Members Using CDP Model in ABAQUS. Advances in Civil Engineering. 2019. 2019(1). Article no. 1745341. DOI: 10.1155/2019/1745341
22. Stoner, J.G. Finite element modelling of GFRP reinforced concrete beams. Computers and Concrete. 2020. 25(4). Pp. 369–382. DOI: 10.12989/cac.2020.25.4.369
23. Metwally, I.M. Three-dimensional nonlinear finite element analysis of concrete deep beam reinforced with GFRP bars. HBRC Journal. 2017. 13(1). Pp. 25–38. DOI: 10.1016/j.hbrcj.2015.02.006
24. Gemi, L., Madenci, E., Özkılıç, Y.O. Experimental, analytical and numerical investigation of pultruded GFRP composite beams infilled with hybrid FRP reinforced concrete. Engineering Structures. 2021. 244. Article no. 112790. DOI: 10.1016/j.engstruct.2021.112790
25. Stoner, J. Finite element modelling of GFRP reinforced concrete beams. MS thesis. University of Waterloo, 2015. DOI: 10.12989/cac.2020.25.4.369

Information about the authors:

Shaysh A. Mohammed,
E-mail: shaysh96@outlook.com

AbdulMuttailb I. Said,
E-mail: dr.abdulmuttalib.i.said@coeng.uobaghdad.edu.iq

Received 15.02.2023. Approved after reviewing 19.10.2023. Accepted 21.10.2023.